Visco-elastic effects on wave dispersion in three-phase acoustic metamaterials

Visco-elastic effects on wave dispersion in three-phase acoustic metamaterials

A.O. Krushynska*, V.G. Kouznetsova, and M.G.D. Geers

Department of Mechanical Engineering, Eindhoven University of Technology, P.O. Box 513, 5600 MB Eindhoven, The Netherlands

Dated: June 28, 2016

Abstract

This paper studies the wave attenuation performance of dissipative solid acoustic metamaterials (AMMs) with local resonators possessing subwavelength band gaps. The metamaterial is composed of dense rubber-coated inclusions of a circular shape embedded periodically in a matrix medium. Visco-elastic material losses present in a matrix and/or resonator coating are introduced by either the Kelvin-Voigt or generalized Maxwell models. Numerical solutions are obtained in the frequency domain by means of $\mathbf{k}(\omega)$-approach combined with the finite element method. Spatially attenuating waves are described by real frequencies ω and complex-valued wave vectors $\mathbf{k}$. Complete 3D band structure diagrams including complex-valued pass bands are evaluated for the undamped linear elastic and several visco-elastic AMM cases. The changes in the band diagrams due to the visco-elasticity are discussed in detail; the comparison between

*Electronic address: akrushynska@gmail.com; Corresponding author

the two visco-elastic models representing artificial (Kelvin-Voigt model) and experimentally characterized (generalized Maxwell model) damping is performed. The interpretation of the results is facilitated by using attenuation and transmission spectra. Two mechanisms of the energy absorption, i.e. due to the resonance of the inclusions and dissipative effects in the materials, are discussed separately.

It is found that the visco-elastic damping of the matrix material decreases the attenuation performance of AMMs; however, if the matrix material is slightly damped, it can be modeled as linear elastic without the loss of accuracy given the resonator coating is dissipative. This study also demonstrates that visco-elastic losses properly introduced in the resonator coating improve the attenuation bandwidth of AMMs although the attenuation on the resonance peaks is reduced.

1 Introduction

Acoustic metamaterials (AMMs) are engineered materials designed to control the propagation of sound and/or elastic waves at subwavelength frequencies. Their functionality originates from local resonances [36, 18, 47, 32, 23] of structural units, usually, periodically arranged. Under certain conditions, AMMs exhibit absolute frequency band gaps, within which the wave propagation is forbidden independent of the wave polarization or wave vector. The band gaps in AMMs are usually opened at low frequencies, for wavelengths of 1-2 orders larger than the spatial period of a periodic metamaterial structure [34, 59, 56, 46, 39, 9]. This fact principally distinguishes AMMs from phononic crystals (PnCs) with band gaps resulting from the Bragg scattering effect [7] for wavelengths in the order of the lattice period. AMMs with local resonances have been widely studied during the past 15 years in view of their potential to demonstrate negative effective properties [35, 58, 61], sub-wavelength imaging and focusing

abilities [33, 30, 29, 31], as well as to perform low-frequency vibration insulation [4, 47], sub-wavelength waveguiding [32, 23], seismic wave protection [6, 9], etc.

To describe the dynamic behavior of AMMs and predict the response of finite-sized structures, it is necessary to solve a dispersion equation relating the wave vector $\mathbf{k}$ of a wave to its frequency ω. For a periodic medium, this equation can be derived by applying the Bloch expansion theorem [5] to a representative unit cell and subsequently solving an eigenvalue problem for ω at specified values of $\mathbf{k}$ or for $\mathbf{k}$ at specified frequencies ω. These two solution techniques are known as $\omega(\mathbf{k})$- or $\mathbf{k}(\omega)$-approaches, respectively [54, 2, 23]. Thus, by analyzing the dynamics of only a single unit cell, both approaches allow constructing a complete band/dispersion diagram including propagating and evanescent waves for an entire infinite periodic medium.

The analysis is commonly performed for propagating waves assuming linear elastic behavior of the material constituents that results in both real-valued frequencies and wave vectors. However, realistic materials such as epoxy and rubber, which are widely used as components of PnCs and AMMs [36, 18, 35, 58, 44, 55, 59, 56, 23, 26], typically reveal a dissipative visco-elastic behavior [17]. In this case, either wave vector or frequency become complex-valued with imaginary parts representing spatial or temporal wave attenuation, respectively [1, 27, 23]. Thus, all the waves become evanescent, and the analysis of complete dispersion diagrams should be performed.

The methods developed to analyze complex-valued dispersion relations can be divided into two groups [2, 23]. The first group deals with real-valued frequencies of harmonic waves and complex-valued wave vectors [40, 42, 60, 38, 44, 16, 2]. This approach is useful for analyzing steady-state wave fields and comparison with experimental data for finite-sized structures. Another group of meth-

ods deals with freely propagating waves possessing complex-valued frequencies, which is relevant for loading conditions of an impulsive nature [45, 19, 20, 48]. The comparison of two mentioned approaches was recently performed and revealed that, for periodic composites with a low up to medium level of dissipation, both approaches provide equivalent results in the long-wavelength range [2].

The effect of material losses on the wave dispersion has been mainly studied for PnCs and less intensively for AMMs. Detailed reviews of the considered dissipative effects and the developed solution methods can be found in the literature [44, 21, 23, 39]. Since this paper deals with visco-elastic effects on wave propagation in solid AMMs of infinite extent, the following brief summary is focusing on the influence of visco-elastic damping on band diagrams.

For PnCs, it has been argued that the visco-elasticity results in shifting pass bands along the frequency axis [42, 19, 20, 44, 2, 21], if the Kelvin-Voigt model or complex-valued elasticity tensor are used to model the damped matrix material. The real part of the wave vector, which describes the propagating part of a wave, appears to be more affected by losses than its imaginary part, especially near the band gap edges [44]. This also causes enhanced wave attenuation near the band gap boundaries, resulting in extension of the effective band gap size for PnCs. For freely propagating waves in PnCs modeled as 1D or 2D mechanical mass-spring systems, it has been also found that the increase of damping leads to broadening of a band gap – a desirable feature for various noise isolation and frequency sensing applications [21, 19].

For AMMs with visco-elastic losses in mass-spring models representing the dynamics of 1D metamaterials, the so-called 'metadamping' phenomenon is discovered, when an AMM exhibits higher levels of dissipation within the propagating modes compared to those for a statically equivalent PnC with identical material damping properties [22]. The parameters of optimal damping ratios are

recently analyzed for 3 simple visco-elastic models: Kelvin-Voigt, Maxwell and standard linear solid-types [39]. The interaction between two attenuation mechanisms, i.e. due to the resonance and dissipative effects, as well as possibilities of tuning the damping to enhance the attenuation bandwidths are thoroughly considered in Refs. [41, 50, 52, 39].

Summarizing, one may conclude that the performed analysis of mechanical mass-spring analogues of 1D AMMs demonstrates that the presence of damping in the resonating units can enhance the performance of metamaterials and provides key attributes for optimal design of dissipative AMMs. However, a systematic study of 2D or 3D configurations of damped continuous AMMs is mandatory in order to understand the wave dispersion mechanism in these structures. Moreover, the realistic visco-elastic behavior of polymers is better described by more complicated visco-elastic models, such as the generalized Maxwell or generalized Kelvin-Voigt models, compared to the simple Kelvin-Voigt model with 1 viscosity parameter not taking into account a spectrum of relaxation times [17]. Thus, it is instructive to investigate whether the phenomena previously found for 1D AMMs with simplified mechanisms of material losses also exist in continuous 2D AMM structures with a sophisticated dissipation. This paper aims at making a step towards achieving the two mentioned objectives.

The goal of this paper is to numerically study the wave dispersion in dissipative solid continuous AMMs, qualitatively compare the obtained wave propagation characteristics with those known for damped PnCs, and identify the role of damping in the metamaterial performance.

To this purpose, we consider an AMM made of 3 material phases in order to analyze separately the effects of material losses in the matrix and coating of resonating units. To minimize computational costs, we consider a 2D configuration consisting of rubber-coated lead cylinders of an infinite length embedded

in an epoxy matrix. The developed solution procedure can be applied to 3D AMMs as well. The material losses are introduced, using a Kelvin-Voigt model with 1 viscosity parameter and a generalized Maxwell model with 8-12 parameters required to represent the experimentally measured behavior of epoxy and rubber polymers [17, 42, 14]. The necessity for considering these two models can be justified as follows. It is known from the study of 1D AMMs that the Kelvin-Voigt-type oscillators provide the best attenuation broadening [39]. This model also allows analyzing the changes in the pass bands location due to various levels of viscosity by varying the value of one relevant parameter. Furthermore, since the Kelvin-Voigt model is often used to represent visco-elastic losses in damped PnCs and AMMs, it seems to be reasonable to evaluate its applicability regions by comparing the attenuation spectra with those calculated with a generalized Maxwell model. As already mentioned, the generalized Maxwell model is often used to fit experimental measurements of storage and loss moduli of polymers [42, 14]. To facilitate the comparison of the complex-valued dispersion spectra and the interpretation of dissipation mechanisms, we use the so-called attenuation spectrum relating the ratio between the imaginary and real parts of the wave vector to the frequency [10, 2]. Finally, the wave transmission analysis is performed to confirm the results obtained for the wave dispersion.

The paper is organized as follows. In Section 2, the problem under consideration is defined in the time domain by using hereditary integrals in linear visco-elastic constitutive relations. The governing equations are then transformed into the frequency domain by means of a combination of the classic correspondence principle and the Laplace-Carson transform. This results in a problem for the corresponding linear elastic medium with frequency-dependent quantities. The evaluation of band diagrams is performed numerically based on

the finite-element method and the $\mathbf{k}(\omega)-$approach to determine the complex-valued wave vectors of spatially decaying waves for fixed values of the frequency. Section 3 presents full complex-valued band diagrams of 2D AMMs for both the undamped linear elastic and damped visco-elastic cases. The resonance and dissipative mechanisms of attenuation are discussed in Section 4. The applicability range of the Kelvin-Voigt model is evaluated by comparing the computed dispersion, attenuation transmission spectra for damped AMMs with those obtained for the generalized Maxwell model. The role of visco-elastic losses in the attenuation performance of damped 2D AMMs is also discussed. The main conclusions are presented in Section 5.

2 Wave propagation in visco-elastic acoustic metamaterials

In this section, we introduce a theoretical approach to evaluate wave dispersion in periodic heterogeneous composites with visco-elastic losses.

Under the assumption that a metamaterial is periodic and of an infinite extent, the analysis of wave dispersion can be restricted to a representative unit cell by applying the Bloch expansion theorem [5]. According to this theorem, the displacement field $\mathbf{u} = u_x\mathbf{e}_x + u_y\mathbf{e}_y + u_z\mathbf{e}_z$ is also periodic (with $(\mathbf{e}_x, \mathbf{e}_y, \mathbf{e}_z)$ vectors of a Cartesian basis) and can be represented in the form of plane waves with wave vector $\mathbf{k} = k_x\mathbf{e}_x + k_y\mathbf{e}_y + k_z\mathbf{e}_z$:

$$\mathbf{u}(\mathbf{x}, \mathbf{k}, t) = \mathbf{U}(\mathbf{x}, \mathbf{k})e^{i(\mathbf{k}\cdot\mathbf{x}-\omega t)}, \tag{1}$$

where $\mathbf{U}(\mathbf{x}, \mathbf{k}) = \mathbf{U}(\mathbf{x} + \mathbf{R}, \mathbf{k})$ is a periodic Bloch displacement vector, $\mathbf{R} = n_x\mathbf{e}_x+n_y\mathbf{e}_y+n_z\mathbf{e}_z$ represents any lattice vector with arbitrary integers n_x, n_y, n_z.

Attention is now focused on steady-state wave propagation at a prescribed

frequency. In this case, the physically realistic scenarios are captured if the frequency ω is assumed to be a real-valued independent variable and the wave vector $\mathbf{k}$ is to be computed [1]. For an undamped medium, there exist real, imaginary and complex values for the wave vector $\mathbf{k}$. Real components of $\mathbf{k}$ are inversely proportional to the wavelength of propagating waves along mutually perpendicular directions. Due to the symmetry of the lattice, these values are restricted to the 1^{st} Brilloiun zone representing a unit cell of the reciprocal lattice-space with the basis vectors $(\mathbf{b}_x, \mathbf{b}_y, \mathbf{b}_z)$ such that $\mathbf{a}\cdot\mathbf{b} = 2\pi\delta_{ij}$ [24]. Pure imaginary components of $\mathbf{k}$ describe standing waves with exponentially decaying or growing amplitudes [2]. These values are not periodic and can take any value from 0 to infinity [44]. Complex-valued components of $\mathbf{k}$ describe propagating waves with attenuating or amplifying amplitudes as the wave progresses within a unit cell. The energy conservation in the lossless elastic medium can be shown by considering complex-conjugate pairs of the wave vector $\mathbf{k}$, which represent two waves propagating in opposite directions and, thus, form a standing wave that, on average, does not transfer any energy. In case of a damped medium, there are no pure real/imaginary nor complex-conjugate wave vectors, but only frequency-dependent complex-valued wave vectors $\mathbf{k}$, the positive imaginary part of which describes wave attenuation due to the material dissipation [16, 44].

The proper statement of the dynamic problem for a linear visco-elastic periodic composite is provided by the standard equation of motion with the classical strain-displacement relation for infinitesimal deformations

$$\nabla \cdot \boldsymbol{\sigma}(\mathbf{x}, t) - \rho(\mathbf{x})\ddot{\mathbf{u}}(\mathbf{x}, t) = \mathbf{0}, \qquad \forall\, t > 0; \tag{2}$$

$$\boldsymbol{\epsilon}(\mathbf{x}, t) = \frac{1}{2}\left(\nabla\mathbf{u}(\mathbf{x}, t) + (\nabla\mathbf{u}(\mathbf{x}, t))^T\right) = \nabla^S\mathbf{u}(\mathbf{x}, t) \tag{3}$$

with the gradient ∇ and symmetric gradient ∇^S operators; $\boldsymbol{\sigma}$ and $\boldsymbol{\epsilon}$ are the

stress and linear strain tensors, respectively; ρ is the material density, and a superimposed dot denotes differentiation with respect to time. Eqs. (2), (3) are supplemented by the visco-elastic stress-strain relation in terms of hereditary or Duhamel integrals [17]:

$$\boldsymbol{\sigma}(\mathbf{x},t) = \int\limits_{-\infty}^{t} K(\mathbf{x},t-\tau)\frac{\partial}{\partial\tau}tr(\boldsymbol{\epsilon}(\mathbf{x},\tau))\mathbf{I}\,d\tau + \int\limits_{-\infty}^{t} 2G(\mathbf{x},t-\tau)\frac{\partial}{\partial\tau}\boldsymbol{\epsilon}^d(\mathbf{x},\tau)d\tau, \quad (4)$$

for the cubical dilatation $tr(\boldsymbol{\epsilon}) = \nabla\cdot\mathbf{u}$ and deviatoric $\boldsymbol{\epsilon}^d = \boldsymbol{\epsilon} - \frac{1}{3}tr(\boldsymbol{\epsilon})\mathbf{I}$ deformations with volumetric $K(t)$ and shear $G(t)$ relaxation moduli, respectively; $\mathbf{I}$ is the second-order unit tensor.

The separation of deformation into two parts, corresponding to a change of volume and a change of shape, appears to be convenient for the description of visco-elastic polymers. The linear visco-elastic behavior of these materials is usually limited to negligibly small volume changes [17, 27]. In this case, $K(t)$ becomes the time-independent equilibrium bulk modulus K. The visco-elastic behavior of polymers is discussed in detail in the next section. To provide a general description of the problem, the bulk relaxation modulus $K(t)$ is considered time-dependent, nevertheless.

By applying the Bloch boundary conditions (1) on the unit cell boundaries and zero initial conditions for the displacements and velocities, the obtained initial-boundary value problem can be formally solved by employing the classic elastic-visco-elastic correspondence principle [1, 27].

To this purpose, the governing equations (2)-(4) are first transformed into the frequency domain by employing the Laplace-Carson transform (LCT), which is s times the Laplace transform:

$$\hat{f}(s) = s\mathcal{L}[f(t)](s) = s\int\limits_{0}^{\infty} f(t)e^{-st}dt, \quad (5)$$

with the complex-valued argument s and transform function $\hat{f}$. The real part of the transform variable s is an abscissa of absolute convergence [57]. It can be set to 0, since the stresses, displacements and strains to be transformed describe real physical quantities, and thus, are absolutely integrable functions in time. The imaginary part of s is assumed to be equal to $i\omega$, corresponding to the harmonic displacement field of the original problem. Hence, the constitutive equation (4) is transformed into the following tensor-form relation between $\hat{\boldsymbol{\sigma}}$ and $\hat{\boldsymbol{\epsilon}}$:

$$\hat{\boldsymbol{\sigma}}(\mathbf{x}, i\omega) = {}^4\hat{\mathbf{D}}(\mathbf{x}, i\omega) : \nabla\hat{\mathbf{u}}(\mathbf{x}, i\omega), \tag{6}$$

where

$${}^4\hat{\mathbf{D}}(\mathbf{x}, i\omega) = \hat{K}(\mathbf{x}, i\omega)\mathbf{II} + 2\hat{G}(\mathbf{x}, i\omega)\left({}^4\mathbf{I}^S - \frac{1}{3}\mathbf{II}\right), \tag{7}$$

where $\mathbf{II}$ is the fourth-order tensor given by $\mathbf{II} = \mathbf{I} \otimes \mathbf{I}$, and ${}^4\mathbf{I}^S$ is the fourth-order symmetric identity tensor.

In order to establish the elastic-visco-elastic correspondence principle [1, 27], let us formulate the corresponding elastic problem for a periodic elastic composite with a representative unit cell of the same configuration and dimensions, which is subjected to the same initial and boundary conditions as the visco-elastic composite. The LCT of the corresponding elastic stress-strain relation is

$$\hat{\boldsymbol{\sigma}}(\mathbf{x}, i\omega) = {}^4\mathbf{D}(\mathbf{x}) : \nabla\hat{\mathbf{u}}(\mathbf{x}, i\omega). \tag{8}$$

The other transformed equations have the same form for the elastic and visco-elastic problems, namely:

$$\nabla \cdot \hat{\boldsymbol{\sigma}}(\mathbf{x}, i\omega) - \rho(\mathbf{x})\omega^2\hat{\mathbf{u}}(\mathbf{x}, i\omega) = \mathbf{0}; \tag{9}$$

$$\hat{\boldsymbol{\epsilon}}(\mathbf{x}, i\omega) = \nabla^S\hat{\mathbf{u}}(\mathbf{x}, i\omega). \tag{10}$$

According to the correspondence principle, the solution of the transformed visco-elastic problem (6), (9), (10) can be obtained from the solution of the transformed corresponding elastic problem (8), (9), (10) replacing $K(\mathbf{x})$ by $\hat{K}(\mathbf{x}, i\omega)$ and $G(\mathbf{x})$ by $\hat{G}(\mathbf{x}, i\omega)$. The correspondence principle holds by virtue of the fact that the Laplace-Carson transform of the visco-elastic constitutive law with convolution integrals (4) is given by the product of the Laplace-Carson transforms of two cumulative functions (8). In relation to the wave propagation in an unbounded medium, the principle enables separating the space and time variables and focusing on the space variation of the wave field at a fixed frequency.

The Laplace-Carson transform is used here instead of the frequently applied Laplace transform [17, 1, 27], since the former allows preserving the same structure of the transformed governing equations as for the elastic case in the time domain and, thus, retaining the physical meaning of the transformed problems. This means that the methods developed to analyze the wave dispersion in periodic composites with linear elastic behavior can be directly applied to visco-elastic composites, taking into account the frequency dependence of the elastic moduli.

In this study, the so-called $\mathbf{k}(\omega)$-approach is used, which is applied in several recent papers to characterize the dissipative behavior of PnCs [44, 16, 8, 2]. In the following, only the key aspects of the approach are outlined by considering a representative unit cell for a two-dimensional periodic medium with spatially dependent material parameters in the (x, y)-plane. By substituting Eqs. (10), (6) into Eq. (9), one obtains the equations governing the wave motion in the unit cell:

$$\nabla \cdot {}^4\mathbf{D} : \nabla \hat{\mathbf{u}}(\mathbf{x}, i\omega) = \rho(\mathbf{x})\omega^2 \hat{\mathbf{u}}(\mathbf{x}, i\omega). \tag{11}$$

Next, the Bloch expansion theorem (1) in the frequency domain takes the fol-

lowing form:

$$\hat{\mathbf{u}}(\mathbf{x}, \mathbf{k}, i\omega) = \hat{\mathbf{U}}(\mathbf{x}, \mathbf{k}, i\omega) e^{i\mathbf{k}\cdot\mathbf{x}}. \tag{12}$$

Thus, the displacement gradient operator becomes:

$$\nabla\hat{\mathbf{u}} = (\nabla\hat{\mathbf{U}} + i\mathbf{k} \otimes \hat{\mathbf{U}}) e^{i\mathbf{k}\cdot\mathbf{x}} = \nabla_{\mathbf{k}}\hat{\mathbf{U}} e^{i\mathbf{k}\cdot\mathbf{x}}. \tag{13}$$

The substitution of the Bloch theorem (12) into the wave equation (11) results in the $\mathbf{k}$-dependent wave equation:

$$\nabla_{\mathbf{k}} \cdot {}^4\mathbf{D} : \nabla_{\mathbf{k}}\hat{\mathbf{U}}(\mathbf{x}, \mathbf{k}, i\omega) = \rho(\mathbf{x})\omega^2\hat{\mathbf{U}}(\mathbf{x}, \mathbf{k}, i\omega). \tag{14}$$

This equation can be solved by means of the finite element method. The discretization of the unit cell into finite elements is performed based on the standard Galerkin approach, which results in the following generalized eigenfrequency equation:

$$(\mathbf{K}(\mathbf{k}, \omega) - \omega^2\mathbf{M})\mathbf{d} = 0, \tag{15}$$

where $\mathbf{d}$ is the column of nodal displacements, $\mathbf{M}$ and $\mathbf{K}(\mathbf{k}, \omega)$ are the mass and stiffness matrices, respectively.

In this work, wave propagation will be restricted to the (x, y) plane with the wave vector $\mathbf{k} = k_x\mathbf{e}_x + k_y\mathbf{e}_y$. Eq. (14) then describes two types of modes. One represents in-plane modes formed by interaction of longitudinal and transverse waves with $\hat{\mathbf{U}} = \hat{U}_x\mathbf{e}_x + \hat{U}_y\mathbf{e}_y$. Another type of modes are out-of-plane modes formed by transverse polarized waves with $\hat{\mathbf{U}} = \hat{U}_z\mathbf{e}_z$. The mass and stiffness matrices are then given by:

$$\mathbf{M} = \sum_e \rho_e \int_{V_e} \mathbf{N}^T\mathbf{N} dV_e; \tag{16}$$

$$\mathbf{K}(\mathbf{k},\omega) = \mathbf{K}_0 - i(k_x\mathbf{K}_1 + k_y\mathbf{K}_2) + k_x^2\mathbf{K}_3 + k_y^2\mathbf{K}_4 + k_xk_y\mathbf{K}_5, \tag{17}$$

where

$$\mathbf{K}_0 = \sum_e \int\limits_{V_e} \mathbf{B}^T\mathbf{D}(\omega)\mathbf{B}dV_e; \tag{18}$$

$$\mathbf{K}_i = \sum_e \int\limits_{V_e} \mathbf{N}^T\mathbf{\Lambda}_i^T\mathbf{D}(\omega)\mathbf{B} - \left(\mathbf{N}^T\mathbf{\Lambda}_i^T\mathbf{D}(\omega)\mathbf{B}\right)^T dV_e, \quad i = 1,2; \tag{19}$$

$$\mathbf{K}_{2+i} = \sum_e \int\limits_{V_e} \mathbf{N}^T\mathbf{\Lambda}_i^T\mathbf{D}(\omega)\mathbf{\Lambda}_i\mathbf{N}dV_e, \quad i = 1,2; \tag{20}$$

$$\mathbf{K}_5 = \sum_e \int\limits_{V_e} \mathbf{N}^T\left(\mathbf{\Lambda}_1^T\mathbf{D}(\omega)\mathbf{\Lambda}_2 + \left(\mathbf{\Lambda}_1^T\mathbf{D}(\omega)\mathbf{\Lambda}_2\right)^T\right)\mathbf{N}dV_e. \tag{21}$$

Here the summation and integration are performed over all the finite elements and the element volume V_e, respectively; $\mathbf{N}$ is the matrix (in-plane modes) or column (out-of-plane modes) of shape functions; $\mathbf{B} = \nabla\mathbf{N}$. The following notations are used for in-plane modes:

$$\mathbf{\Lambda_1} = \begin{bmatrix} 1 & 0 \\ 0 & 0 \\ 0 & 1 \end{bmatrix}, \quad \mathbf{\Lambda_2} = \begin{bmatrix} 0 & 0 \\ 0 & 1 \\ 1 & 0 \end{bmatrix}, \quad \mathbf{D} = \begin{bmatrix} \hat{K} + \frac{4\hat{G}}{3} & \hat{K} - \frac{2\hat{G}}{3} & 0 \\ \hat{K} - \frac{2\hat{G}}{3} & \hat{K} + \frac{4\hat{G}}{3} & 0 \\ 0 & 0 & \hat{G} \end{bmatrix} \tag{22}$$

and, for out-of-plane modes:

$$\mathbf{\Lambda_1} = \begin{bmatrix} 1 \\ 0 \end{bmatrix}, \quad \mathbf{\Lambda_2} = \begin{bmatrix} 0 \\ 1 \end{bmatrix}, \quad \mathbf{D} = \hat{G}(\mathbf{x}, i\omega). \tag{23}$$

In the matrix $\mathbf{D}$, the dependence of the elastic moduli $\hat{K}(\mathbf{x},\mathbf{i}\omega)$ and $\hat{G}(\mathbf{x},\mathbf{i}\omega)$ on the spatial coordinates and frequency is omitted for brevity.

Since the elastic moduli entering $\mathbf{D}$ are frequency-dependent, one assumes that the frequency ω is specified, whereas (real, imaginary or complex) k_x and

k_y are unknown. Thus, the problem (15) for the eigenfrequencies should be reformulated as an eigenvalue problem for the wave vector $\mathbf{k}$. This can be performed by specifying a relation between the wave vector components, *e.g.*, $k_y = ck_x$ as in Ref. [2], where c is a real constant. By inserting this relation into Eq. (15) and reformulating the problem into the first-order form, one obtains [2]:

$$(\overline{\mathbf{K}}(\omega) - k_x\overline{\mathbf{M}})\overline{\mathbf{d}} = 0 \tag{24}$$

with

$$\overline{\mathbf{K}} = \begin{bmatrix} \mathbf{I} & \mathbf{0} \\ -i\left(\mathbf{K}_1 + c\mathbf{K}_2\right) & \mathbf{K}_0 - \omega\mathbf{M} \end{bmatrix}, \quad \overline{\mathbf{d}} = \begin{bmatrix} \mathbf{d} \\ k_x\mathbf{d} \end{bmatrix}; \tag{25}$$

$$\overline{\mathbf{M}} = \begin{bmatrix} \mathbf{0} & \mathbf{I} \\ -\left(\mathbf{K}_3 + c\mathbf{K}_5 + c^2\mathbf{K}_4\right) & \mathbf{0} \end{bmatrix}. \tag{26}$$

Eq. (24) can be solved for specified frequencies ω and periodic boundary conditions for $\overline{\mathbf{d}}$ on the unit cell boundaries. The computed eigenvalues are used for constructing a dispersion spectrum (band diagram) along lines $k_y = ck_x$ for fixed values of c through the 1st Brillouin zone ($c = 0$ for $\Gamma - X$ direction, $c = 1$ for $\Gamma - M$ direction, etc.). The eigenvalues for the linear elastic and viscoelastic cases are calculated and validated with data available in the literature for phononic crystals [44, 2]. The results calculated for the adopted discretization agree well with those for a refined mesh, confirming the mesh-independence and stability of the calculations.

The transmission of the wave field in a finite-size metamaterial is analyzed by using the commercial software COMSOL Multiphysics 5.0. The calculations are performed in the frequency domain for structures composed of 10 representative unit cells arranged along the horizontal direction. The structure isassumed to

be infinite in the vertical direction, which is modeled by periodic (continuity) boundary conditions at the horizontal bottom and top boundaries. A plane wave of amplitude 1e-3 (polarized vertically or horizontally) is incident on the left vertical boundary of the structure, while a non-reflecting boundary condition (PML with default characteristics) is applied on the right boundary. The frequency is swept in 100 steps within the ranges specified for each considered case by the corresponding dispersion spectrum. The transmitted wave field is represented by the averaged total displacements over the last 5 unit cells of the considered finite AMM structure.

3 AMM composition and visco-elastic models

3.1 The AMM configuration

This paper deals with an AMM made of infinite rubber-coated lead cylinders of circular cross-section embedded in epoxy in a periodic square lattice. The representative unit cell of the metamaterial is shown in Fig. 1 together with the corresponding unit cell in the reciprocal space (the 1^{st} Brillouin zone). The described AMM exhibits subwavelength band gaps originating from local resonances [36, 35, 59, 26, 23]. When material losses are considered, this 3-component configuration allows studying separately the influence of damping in the matrix and/or coating materials on the dispersion and attenuation characteristics of the elastic waves.

The radius of the lead inclusion is 5 mm, the coating thickness is 2.5 mm, and the unit cell size is 21 mm. The filling fraction of inclusions, defined as the ratio between the coated inclusion area to the area of the unit cell, is 40%. The low filling fraction is chosen to eliminate interactions between inclusions, which may lead to a complex behavior of the dispersion curves [26]. The elastic

Table 1: Material properties for the linear elastic constituents of AMMs considered in this work (bulk modulus K^*, shear modulus G^*, density ρ, longitudinal c_l and shear c_s wave velocities)

Material	K^* (Pa)	G^* (Pa)	ρ (kg/m^3)	c_l (m/s)	c_s (m/s)
Lead [36]	5.23×10^{10}	1.49×10^{10}	11600	2490	1133
Epoxy [14]	3.1×10^{9}	7.9×10^{8}	1200	1860	810
Rubber [42]	1.83×10^{9}	7.1×10^{5}	1260	1200	24

properties of the constituent materials are given in Table 1. Lead is assumed to be isotropic and lossless, whereas epoxy and rubber are modeled as either linear elastic or linear visco-elastic materials with parameters discussed in the next section.

3.2 Visco-elastic models

To solve the eigenvalue problem (24), the mathematical expressions for the frequency dependent bulk $K(i\omega)$ and shear $G(i\omega)$ moduli are required. Prior to the introduction of these relations, it should be noted that under isothermal conditions the bulk modulus of most polymers can be well approximated by a constant time-independent equilibrium value $\hat{K} = K^*$ over a wide range of time scales [17, 12]. The physical explanation for this originates from the molecular structure of the polymers, resulting in a visco-elastic movement of polymer chains in response to shear a stress, while under hydrostatic stress only local motion of molecules takes place, which is not influenced by long range entanglements and cross-links [28, 49]. As a result, the relaxation times of the volumetric response are considerably shorter than those of the shear response, and the volumetric excitation attains equilibrium relatively fast [13]. Therefore, the bulk modulus of most dense polymers can be assumed constant within the limits of linear visco-elasticity. A frequency-independent value K^* is therefore adopted, which is equal to that of the linear elastic case, given in Table 1.

Table 2: Storage modulus G' and viscosity G'' values for the visco-elastic material behavior described by the Kelvin-Voigt model (27)

Material	G' (Pa)	G'' (Pa·s)		
Epoxy	7.9×10^8	1e4	5e4	1e5
Rubber	7.1×10^5	5	10	25

The frequency dependence of the shear modulus $\hat{G}(i\omega)$ can be effectively approximated by exploiting various mechanical models with elastic (springs) and viscous (dashpots) elements [17, 27]. In this study, two mechanical models are considered.

The first model is a simple Kelvin-Voigt model represented by a spring parallel to a dashpot. For a harmonic wave field, the Kelvin-Voigt model provides a complex-valued shear modulus with imaginary part linearly proportional to the frequency:

$$\hat{G}(i\omega) = G' + i\omega G''. \tag{27}$$

The spring element has a stiffness value equal to the real part G', also called storage modulus, whereas the frictional resistance of the dashpot yields the to viscosity contribution G''. To evaluate the influence of various levels of viscosity on the wave propagation characteristics, different viscosity values for epoxy and rubber are considered as given in Table 2. The choice of these values is discussed in the next section.

The Kelvin-Voigt model is practically not very useful, since its simplicity prohibits a reliable fit of experimental data. However, this model has been used before in theoretical studies of the material damping effects on dispersion characteristics of PnCs, e.g. [2, 44, 23], since it enables analyzing gradual changes in pass bands behavior by progressively varying the viscosity G''.

The second model is a generalized Maxwell model, which takes into account

a spectrum of relaxation times of a visco-elastic medium. The model can be represented by a parallel configuration of different Maxwell elements (a spring and a dashpot in series) with an extra parallel spring to describe the long-term behavior of a visco-elastic medium [27]. For an n-element generalized Maxwell model, the shear modulus is calculated as follows:

$$\hat{G}(i\omega) = G_\infty + \sum_{i=1}^{n} \frac{i\omega G_i}{i\omega\tau_i + 1}, \tag{28}$$

where τ_i and G_i are the relaxation times and corresponding relaxation shear moduli of the Maxwell elements, and G_∞ is the equilibrium shear modulus. The number n is usually chosen on the basis of an adequate fit of experimental data.

The generalized Maxwell model is often used to characterize the experimentally measured behavior of linear visco-elastic materials by performing dynamic mechanical analysis (DMA). It has been recently found that dynamic torsion experiments on long rods are the most direct and reliable methods for determining the time-dependent shear modulus [12]. In the present work, the visco-elastic behavior of epoxy is described by a set of relaxation pairs (G_i, τ_i) given in Table 3. These data are obtained by fitting dynamic torsion measurements for the storage and loss moduli of the epoxy bars under isothermal conditions [14]. The small strain elastic behavior of the material at room temperature with $\nu = 0.38$ is recovered by combining the elastic bulk modulus K^* with the high glassy shear modulus $G^* = G_\infty + \sum_{i=1}^{n} G_i$. The equilibrium shear modulus G_∞ is used to recover the finite strain behavior at high temperatures with $\nu = 0.5$ [14].

Unfortunately, a similar complete data set for the visco-elastic behavior of rubber is not reported in Ref. [14]. Standard uniaxial tension or compression tests are commonly performed, whereas visco-elastic data in shear hardly appears in the literature [12]. For this reason, the experimental data for dynamic

tension test on a commercial silicone rubber reported in Ref. [42] is here used instead. This type of experiment provides a time-dependent Young's modulus, which is often used to estimate the shear and compression response by assuming a constant Poisson's ratio through the following approximation [42, 12, 15]:

$$G(t) \approx \frac{E(t)}{2(1+\nu)}, \quad K(t) \approx \frac{E(t)}{3(1-2\nu)}. \tag{29}$$

However, this approximation appears to be rather inaccurate, since it is well-known that the Poisson's ratio of many polymers also depends on loading time [25, 27, 12]. Furthermore, it has been shown that the standard measurement accuracy is totally inadequate to convert the Young's modulus functions into the other material moduli, since the relative error, especially for the bulk modulus, is extremely sensitive to the errors in the material functions $E(t)$ and $\nu(t)$ [11, 37, 49, 53].

Based on this understanding, the visco-elastic properties of the rubber are extracted from the experimental measurements in Ref. [42] in the following way. The first step was to evaluate the equilibrium shear modulus G_∞, for which the approximation $G_\infty = \frac{E_\infty}{2(1+\nu_\infty)}$ can be assumed. To this purpose, the Poisson's ratio was determined from the relation $\nu_\infty = \frac{M_\infty - 2G'_\infty}{2M_\infty - 2G'_\infty}$ with longitudinal modulus $M_\infty = \rho c_l^2$ and shear modulus $G'_\infty = \rho c_s^2$ [51]. The estimated $\nu_\infty = 0.49986$ indicates that the polymer is in the rubbery state. Thus, the corresponding elastic behavior can be recovered for $G_\infty = G^*$ by setting $G_i = 0$ for $i = 1, ..., n$ in relation (28). The obtained $G_\infty = 71$ kPa corresponds to $c_s \approx 24$ m/s, which is slightly higher than $c_s \approx 20$ m/s (corresponding to $G'_\infty = 50.4$ kPa). Note that the value of G'_∞ used here only serves to estimate the Poisson's ratio of the rubber in the equilibrium state, since the corresponding shear velocity c_s was not measured experimentally, but taken from the literature as an average value for various types of rubber [42]. The relaxation shear moduli G_i were

Table 3: Generalized Maxwell model relaxation times τ_i and associated shear moduli G_i for epoxy (12DA3) [14] and rubber (commercial silicone elastomer) [42]

Epoxy		Rubber	
τ_i (s)	G_i (Pa)	τ_i (s)	G_i (Pa)
0.3031×10^{-4}	0.1476×10^{9}	4.32×10^{-9}	3.0003×10^{6}
0.1721×10^{-3}	0.1756×10^{9}	5.84×10^{-8}	1.4001×10^{6}
0.9768×10^{-3}	0.2025×10^{9}	3.51×10^{-7}	9.8009×10^{5}
0.5545×10^{-2}	0.1775×10^{9}	2.28×10^{-6}	8.0341×10^{5}
0.3147×10^{-1}	0.6802×10^{8}	1.68×10^{-5}	6.2339×10^{5}
0.1787×10^{0}	0.1139×10^{8}	2.82×10^{-4}	4.3671×10^{5}
0.1014×10^{1}	0.2264×10^{7}	7.96×10^{-3}	2.3402×10^{5}
0.5757×10^{1}	0.8132×10^{6}	9.50×10^{-3}	1.4835×10^{5}
0.3268×10^{2}	0.4020×10^{6}		
0.1855×10^{3}	0.1760×10^{6}		
0.1053×10^{4}	0.5056×10^{5}		
0.5977×10^{4}	0.1265×10^{5}		

calculated by means of the relation $G_i = \frac{E_i}{2(1-\nu_\infty)}$ and given in Table 3. Since, as mentioned above, this is a debatable approximation, the results obtained by means of this data set should not be considered as quantitative and only provide a qualitative description of the wave dispersion in the visco-elastic rubber.

4 Results and discussion

This section presents complete band diagrams for AMMs with undamped and damped components and discusses the influence of the visco-elastic matrix and/or coating behavior on the dispersion and attenuation of elastic waves. Furthermore, the ability of the Kelvin-Voigt model with one viscosity parameter to predict the wave dispersion in visco-elastic AMMs is evaluated compared to the generalized Maxwell model, which takes into account a number of relaxation times and corresponding relaxation moduli fitting the experimental data.

The band structures are computed for the $\Gamma - X$ direction within the irre-

ducible Brillouin zone (see Fig. 1c, i.e. $k_y = ck_x = 0$, $c = 0$). The eigenvalue problem (24)-(26) for wave number k_x was solved for discrete values of the frequency in a selected range. The unit cell shown in Fig. 1b was discretized into 7148 2D quadrilateral 8-node finite elements. The vertically (out-of-plane) and horizontally (in-plane) polarized modes are considered separately. First, the out-of-plane modes are investigated, the dispersion of which is governed by only the shear modulus G resulting in simple band structure diagrams (see, e.g. Ref. [26]). The analysis of out-of-plane modes in a damped AMM enables selection of the values of the viscosity parameter in the Kelvin-Voigt model for both epoxy and rubber, which are further used for studying visco-elastic effects on the wave dispersion of in-plane modes.

The band structures are presented through 3D diagrams along with their corresponding 2D projections on the real- and imaginary-valued planes of the normalized wave number $k_x a/2\pi$. In the band diagrams, the real parts of the wave number slightly exceed the range of the Brillouin zone in order to emphasize the periodicity of the dispersion curves. As the imaginary part of the wave number is non-periodic, only those imaginary- and complex-valued curves are shown that intersect pass bands of propagating waves (for the reference linear elastic case) in the considered frequency range. The considered values of frequencies are limited up to those of the second band gap. To facilitate the interpretation of the wave dispersion and compare results for damped and undamped cases, we also use the so-called attenuation diagrams plotting the ratio between the imaginary and real pars of the wave number $\eta = \frac{2\mathrm{Im}k_x}{\mathrm{Re}k_x}$ versus the wave frequency $f = 2\pi\omega$ [10, 2].

4.1 Undamped linear elastic AMM

The 3D and 2D band structure diagrams for the out-of-plane modes in the linear elastic material are shown in Fig. 2 a-b with a band gap between 543 Hz and 1041 Hz shaded in gray. The band diagram consists of two curves indicated by numbers, each of them spanning continuously the whole considered frequency range starting from 0. This structure satisfies the continuity condition for dispersion curves and confirms the completeness of the dispersion spectrum from the mathematical point of view [43].

From the physical point of view, there are two pass bands with real-valued wave numbers (shown by blue) corresponding to propagating waves. They exist only outside the band gap. The lowest pass band contains a horizontal part representing a localized mode, at which the motion of the lead core occurs out-of-phase to the motion of the matrix material [36, 26]. This mode opens a band gap, which is also known as a hybridization band gap [32]. The band gap is recognized as local resonance due to the fact that the Bloch wave vector $k_x a$ experiences a π jump for its real part inside the band gap and shows an abrupt change in the slope of its imaginary part in the vicinity of the frequency for the localized mode. This behavior has been previously observed for lumped 1D AMMs and is in a striking contrast to the dispersion curve behavior typical for Bragg band gaps [59].

The band structure diagram for in-plane modes with a band gap between 2892-3720 Hz is shown in Figs. 2 d-e and is more complex, since it contains more dispersion curves. However, all the features found for the out-of-plane modes can be observed for the in-plane modes as well. In particular, each mode spans the whole frequency range by starting from the zero frequency and consists of different branches corresponding to propagating and evanescent waves. The symmetry with regard to the first Brillouin zone's border is preserved for the

curves with real wave numbers. The lower bound of the band gap is again formed by a localized mode, and the behavior of the dispersion curves shows that the band gap is of a hybridization nature as described above. Note that the localized modes at frequencies 912 Hz and 4876 Hz corresponding to torsional motions within the inclusions [26] are badly resolved, as the $\mathbf{k}(\omega)$-approach used to evaluate the band structure is insensitive to uncoupled localized modes.

The attenuation spectra for the out-of-plane and in-plane modes are shown in Figs. 2c and f, respectively. From the definition of η is obvious that the attenuation for real-valued branches is zero. Hence, for an undamped AMM, the attenuation outside a band gap always equals to zero. Within the band gaps, the value of η is unbounded for pure imaginary branches and takes finite values for complex branches.

It is important to emphasize here that for the linear elastic material, the wave attenuation solely occurs due to the local resonance effect without any damping in the material constituents. Therefore, when analyzing visco-elastic AMMs, this pure resonance contribution can be 'subtracted' from the attenuation obtained for a damped AMM, yielding attenuation values due to the visco-elastic effect only. This distinction allows quantifying the influence of various mechanisms of the wave attenuation on the AMM performance.

4.2 Visco-elastic AMMs

The wave attenuation performance of dissipative AMMs is evaluated by using the Kelvin-Voigt (27) and generalized Maxwell (28) models for dissipative matrix and/or coating materials. First, we study the effect of the viscosity parameter G'' (Kelvin-Voigt model) on the wave dispersion in the so-called 'empty-lattice' material, which is continuous homogeneous material artificially divided into a square lattice of unit cells with Bloch boundary conditions at each unit cell [44,

55]. Figs. 3 a-b show 2D dispersion spectra for empty-lattice visco-elastic epoxy and rubber materials, respectively, for 4 different arbitrary chosen values of G''. The spectra are calculated for the same frequency range and unit cell size as for the linear elastic AMM described above. It is evident that the imaginary part of the wave vector is more influenced by the viscosity compared to the real part, as for any homogeneous visco-elastic medium [1, 3]. The shear wave velocity in rubber has a rather low value (see Table 1) resulting in folding of the dispersion curves at the boundary of the IBZ at the considered frequencies. The indicated viscosity values are further used to analyze the changes in the band diagrams for visco-elastic AMMs compared to the reference linear elastic case.

4.2.1 Visco-elastic AMM with a damped matrix

Figs. 4 a-b present the dispersion spectrum for the out-of-plane modes in the visco-elastic AMM with a mildly damped epoxy ($G'' = 1e4$ Pa·s, blue lines) compared to the undamped linear elastic AMM ($G'' = 0$, black lines). Obviously, there are no apparent differences between the real branches for both cases; the imaginary branch corresponding to the visco-elastic AMM becomes complex-valued right at the lower boundary of the band gap for certain wave numbers; the complex-valued curve located exactly at the Brillouin zone border for the undamped AMM is divided into 2 symmetric curves and undergoes the same twisting as the imaginary curve. The mentioned changes are hardly noticable in the 2D representation of the spectrum in Fig. 4 b, but are clearly observed in the 3D plot in Fig. 4 a. The corresponding attenuation spectrum is shown in Fig. 4 c. Even though all the waves become evanescent in visco-elastic AMMs, the introduction of a small viscosity in the matrix material does not substantially alter the wave attenuation performance of AMM due to the local resonance effect. In this sense, the wave dispersion in visco-elastic AMMs qualitatively differs from that for PnCs, for which the edges of band gaps become

rounded even for small viscosity levels [44].

Next, the viscous parameter is further increased up to $G'' = 5e4$ Pa·s and $G'' = 1e5$ Pa·s (light blue and green lines in Figs. 4 d-e, respectively). The trends observed for a lower value of G'' become naturally more pronounced, and the two complex branches lying within the IBZ approach each other for higher viscosity values. It is further observed that the effect of the viscosity is larger on the imaginary part of the wave vector similarly to the case of homogeneous materials [1, 3]. The real part is only slightly influenced at higher frequencies, as the viscosity value for the shear modulus G increases linearly with frequency (cf. Eq. (27)). This observation is in striking contrast to the behavior of PnCs with a damped matrix, for which the visco-elasticity influences mostly the real part of the wave vector and causes the rounding of the edges of the band gap bounds [44].

The attenuation spectrum for higher values of G'' presented in Fig. 4 f reveals that the band gap frequencies are almost not affected; however, within the band gap, the wave attenuation decreases as the viscosity level increases. The decrease of the wave attenuation occurs due to the fact that by introducing viscosity in the matrix material, the pure imaginary dispersion branch, which represents a non-propagating wave (black curve, $G'' = 0$), is transformed into a propagating complex-valued mode, the spatial attenuation of which is characterized by a small value of the imaginary part of the wave vector. As the damping increases, the imaginary value decreases. This naturally leads to the conclusion that an increasing visco-elastic behavior of the matrix material decreases the attenuation performance of the acoustic metamaterial.

Red curves in Fig. 4 d-e show the dispersion spectrum for a visco-elastic AMM with the damped matrix modeled by the generalized Maxwell model, the parameters for which taken from experimentally measured data (Table 3). From

the comparison of this spectrum with the two spectra constructed by using the Kelvin-Voigt model, it can be found that, in general, a Kelvin-Voigt model, with a properly assigned viscosity value, well represents the wave dispersion in an AMM with a damped matrix. Essential deviations between the two models are observed only in the very low frequency range (up to 200 Hz), where the complex curve described by the Maxwell model has a pronounced curving. However, since these frequencies are significantly below the band gap, the evaluation of the AMM performance at those frequencies is not of a critical importance. These discrepancies can be ignored. Hence, one can conclude that outside the band gap, the wave attenuation performance of AMM due to the visco-elastic effect in the matrix material increases linearly with the frequency in the same way as in homogeneous visco-elastic solids.

The conclusions derived above remain valid for in-plane modes as well. Figs. 5 a,b present the 3D dispersion and attenuation spectra, respectively, for a dissipative AMM with viscosity parameters $G'' = 1e2$ Pa·s and $G'' = 1e3$ Pa·s for the visco-elastic epoxy matrix. Smaller values of the viscosity (compared to those for the out-of-plane modes) are chosen, since for higher values the matrix appeared to be too damped that was indicated by the presence of a large number of additional complex branches, resulting in an almost uniform damping over the whole considered frequency range and leading to the disappearance of the band gap.

In general, all the trends in the dispersion and attenuation curves discussed for the out-of-plane modes are observed for the in-plane modes. However, the conclusion on the negative effect of damping on the AMM performance cannot be directly derived from the dispersion spectrum for the in-plane modes, since the behavior of the curves is more complicated. To justify this conclusion, we evaluated the transmission displacement field for waves propagating in hor-

izontal (x-axis) and vertical (y-axis) directions. The normalized (with regard to the amplitude of an incident wave) simulation results are shown in Fig. 5 c and d around the band gap frequencies, respectively. For horizontally polarized waves (Fig. 5c), the differences between elastic and visco-elastic structures are observed only outside the band gap, and they do not appear for even medium values of viscosity. At the same time, a decrease of the attenuation level within the band gap is clearly observed for vertically polarized waves (Fig. 5d), while increasing the viscosity level.

Therefore, a small level of the visco-elastic dissipation in the matrix material does not affect the AMM performance, and the matrix behaves as a linear elastic material within the band gap. Contrary to this, medium damping results in a decline of the wave attenuation performance and should be either avoided or minimized.

4.2.2 Visco-elastic AMM with a damped coating

The complete dispersion diagram for out-of-plane modes in the AMM with a dissipative coating, $G'' = 5$ Pa·s, is shown in Figs. 6 a-b (blue lines) together with the reference diagram for the undamped case (black lines). For this low viscosity level, the wave propagation in homogeneous rubber appears to be only slightly damped at higher frequencies as illustrated in Fig. 3 b. However, the band diagram of the dissipative AMM is changed significantly compared to the reference linear elastic AMM that is in contrast to the case of a damped matrix, see Figs. 4 a-b.

The most striking difference is the disappearance of the horizontal part of the real-valued branch corresponding to the localized mode, with forms the lower band gap bound in the linear elastic AMM. The branch becomes complex-valued with large imaginary part. The dispersion diagram for the dissipative visco-elastic AMM has still two dispersion curves, as in the linear elastic case.

However, the trends of these branches differ significantly that also leads to the formation of the so-called 'wavenumber' band gap [16, 20], i.e. a wavenumber range with no propagating waves. The dispersion curve 2 in the visco-elastic case is formed by only complex-valued branches with large imaginary parts. Most probably, this curve is responsible for the occurrence of the 'metadamping' phenomenon in AMMs [22], i.e. enhanced attenuation performance of AMMs compared to the statically equivalent PnC configurations. (Note that all the mentioned differences are not visible in the 2D representation of the band diagram, Fig. 6 b.) The analysis of the attenuation spectrum in Fig. 6 c shows that additional wave attenuation occurs near the band gap edges. The physical reason for this enhanced dissipation, as discussed in Ref. [39], is a higher velocity of waves in the visco-elastic coating resulting in a faster response of the resonator at near-resonant frequencies.

As the viscosity level is increased up to $G'' = 10$ Pa·s or $G'' = 25$ Pa·s, the above mentioned trends in the wave dispersion changes are amplified as shown in Figs. 6 d-e in light-blue and green. For various viscosity levels, the horizontal part of the complex-valued branch has the same frequency as the lower bound of the band gap in the linear elastic case. The attenuation rate η shown in Fig. 6 f indicates that the increase of damping diminishes the attenuation within the band gap. The value η, which is unbounded at the lower band gap bound due to undamped resonances of inclusions in the linear elastic case, becomes finite and is shifted towards higher frequencies. The clear bounds of the band gap (as in the linear elastic case) are smeared out with increasing viscosity. Thus, without a reference solution for the undamped AMM, it would be difficult to identify the frequency band gap. However, additional dissipation of the propagating modes results in a wider attenuation spectrum for the visco-elastic AMM. Thus, optimal choice of damping for the coating material, similar to that proposed

for a mass-spring analogue of 1D AMM [39], may substantially increase the attenuation performance of damped AMMs.

The band diagram for the damped AMM with visco-elastic rubber represented by the generalized Maxwell model is shown in Figs. 6 d-e by red curves. Again, as in the case of the AMM with a dissipative matrix, the behavior of the dispersion curves evaluated for the two visco-elastic models is qualitatively similar, except at low frequencies. However, for the generalized Maxwell model, the curve bends are shifted towards higher frequencies compared to those for the Kelvin-Voigt model. The same conclusion can be derived from the analysis of the attenuation spectrum in Fig. 6 f in comparison with those for the Kelvin-Voigt model. The observed shift of the band gap is most probably due to the inaccurate approximation of visco-elastic parameters for rubber as discussed previously.

Figs. 7a,b show dispersion and attenuation spectra for in-plane modes in a damped AMM (dark and light blue curves) along with those for the undamped AMM (black curves). The viscosity parameters are $G'' = 5$ Pa·s (dark blue) and $G'' = 10$ Pa·s (light blue) in the Kelvin-Voigt model for the visco-elastic rubber. The visco-elastic effects on the wave dispersion discussed above for the out-of-plane modes are found for in-plane modes as well despite the more complicated behavior of the in-plane dispersion curves. The calculations performed for the generalized Maxwell model are not shown here to keep the figures clear. However, the same shift of the band gap frequencies to higher frequencies as described for out-of-plane modes is observed.

The main conclusion that a visco-elastic behavior of the coating material results in extending the band gap size with simultaneous decrease of the wave attenuation within the band gap is confirmed by the transmission analysis for horizontally and vertically polarized in-plane waves as shown in Fig. 7c and d,

respectively.

4.2.3 Visco-elastic AMM with damped matrix and coating

Finally, we analyze a dissipative AMM with both visco-elastic matrix and coating and compare the resulting dispersion and attenuation spectra with those considered in the two previous sections.

Although the calculations have been performed for both mode types and the two analyzed visco-elastic models, we discuss here only the out-of-plane modes in a damped metamaterial with experimentally measured visco-elastic losses represented by the generalized Maxwell models (Table 3). The corresponding band structure and attenuation diagrams are shown in Fig. 8 by light green lines; blue and orange lines indicate diagrams for the AMMs with only dissipative matrix or coating materials, respectively. At frequencies below the band gap, the wave attenuation occurs purely due to visco-elasticity of the matrix material. This is due to the fact that the appropriate wavelengths of waves propagating in the matrix are 2 orders of magnitude larger than the resonator size, and as the filling fraction for the inclusions is rather low, the waves do not 'feel' its presence. However, starting from frequencies slightly below the band gap and up to the highest considered frequency, the wave dispersion and attenuation are governed solely by visco-elastic damping in the coating material, and the damping in the matrix is not pronounced anymore.

Therefore, for the evaluation of the wave attenuation performance of 3-phase AMMs made of visco-elastic polymers, the matrix material (if not too damped) can be modeled as a linear elastic material to reduce the computational costs. Visco-elastic losses in the coating should be properly accounted for, in any case.

5 Conclusions

This paper analyzed the wave dispersion properties and attenuation performance of continuous dissipative AMMs with local resonators. The metamaterial configuration consists of coated inclusions of infinite length placed in a periodic square array in the matrix material. The visco-elastic losses in the matrix or/and coating materials were separately considered for out-of-plane and in-plane elastic waves, propagating in a 2D structure without mutual interactions. The solution for both wave types was obtained by means of the finite element method in the frequency space for a representative unit cell. The dispersion of spatially decaying waves described by complex-valued wave numbers was evaluated by solving the dispersion equation for fixed real-valued frequencies. In this way, the complete band structure diagrams were constructed for both linear elastic and visco-elastic AMM materials.

Two mechanisms contributing to wave attenuation in damped AMMs were analyzed separately. The first mechanism, originating from local resonances of the inclusions, is responsible for the existence of subwavelength band gaps. The second mechanism appears by introducing visco-elastic losses in the matrix and/or coating materials. The visco-elasticity was modeled by either a Kelvin-Voigt model, which is frequently used to study damped metamaterials, or by a generalized Maxwell model, representing real visco-elastic behavior of polymers.

The main effects of the material visco-elasticity on the wave attenuation performance of AMMs are as follows:

- A small amount of visco-elastic damping in the matrix influences mostly pure imaginary and complex branches of the dispersion curves similarly to homogeneous materials (Figure 4), which is in contrast to damped PnCs [44]. As the viscosity level increases, the visco-elastic matrix deteriorates the attenuation performance of AMMs (Figure 5).

- For a low to medium damped coating, the attenuation around the band gap edges increases, although the peak of the resonance attenuation inside the band gap decreases (Figures 6 and 7). This agrees with the conclusions derived for the mass-spring analogues of 1D AMMs [39].

- If the damping is present in both the matrix and coating material, the wave dispersion below the lowest band gap is governed purely by the visco-elasticity of the matrix, whereas near the band gap and at higher frequencies only the visco-elasticity of the coating dominates (Figure 8).

From the results of the transmission analysis, it can be concluded that a medium level of damping present in *any* constituent of a three-phase AMM results in decreasing the wave attenuation performance of the AMM (Figures 5c,d and 7c,d). This important conclusion contradicts the common expectations that regardless of the level of damping in any material component, an increased dissipation response is expected. However, the dissipative coating material allows extending the band gap size that might be useful for practical applications of AMMs. The slightly damped matrix can be modeled as linear elastic provided the visco-elastic losses in the coating are properly taken into account (Figures 5c,d and 8).

Finally, from the comparison of the two visco-elastic models, i.e. Kelvin-Voigt and Maxwell, it follows that the Kelvin-Voigt model provides reliable results concerning the wave dispersion, except for low frequencies. This model can be efficiently used for analyzing realistic AMMs possessing unavoidable intrinsic losses, if the viscosity parameter for a given material is chosen in the correct range.

The performed study of the wave dispersion in visco-elastic AMMs reveals that a proper combination of the local resonance effect and material dissipation can be efficient in tailoring the absorption properties of AMMs. This may enable

design of practical systems with effective damping and stiff structural properties suitable for various engineering applications.

References

[1] J.D. Achenbach. *Wave propagation in elastic solids.* Amsterdam: North-Holland, 1973.

[2] E. Andreassen and J.S. Jensen. Analysis of phononic bandgap structures with dissipation. *ASME J. Vibr. Acoust.*, 135:041015, 2013.

[3] B.A. Auld. *Acoustic fields and waves in solids.* Wiley: New York, 1973.

[4] E. Baravelli and M. Ruzzene. Internally resonating lattices for bandgap generation and low-frequency vibration control. *J. Sound Vibr.*, 332:6562–6579, 2013.

[5] F. Bloch. *Über* die Quantenmechanik der Elektronen in Kristallgittern. *Zeitsch. Phys.*, 52:555–600, 1929.

[6] S. Brûle, E. Javelaud, S. Enoch, and S. Guenneau. Experiments on seismic metamaterials: molding surface waves. *Rhys. Rev. Lett.*, 112:133901, 2014.

[7] L. Brillouin. *Wave propagation in periodic structures.* Dover, New York, 1946.

[8] M. Collet, M. Ouisse, M. Ruzzene, and M.N. Ichchou. Floquet-Bloch decomposition for the computation of dispersion of two-dimensional periodic damped mechanical systems. *Int. J. Solids Struct.*, 48:2837–2848, 2011.

[9] A. Colombi, P. Roux, S. Guenneau, and R. Matthieu. Directional cloaking of flexural waves in a plate with a locally resonant metamaterial. *J. Acoust. Soc. Am.*, 137:1738, 2015.

[10] L. Cremer, M. Heckl, and B.A.T. Petersson. *Structure-borne sound*. Springer, Berlin Heidelberg, 2005.

[11] R.J. Crowson and R.G.C. Arridge. Linear viscoelastic properties of epoxy resin polymers in dilatation and shear in the glass transition region. 1. Time-temperature superposition of creep data. *Polym. J.*, 20:737–746, 1979.

[12] J. de Vreugd. *The effect of aging on molding compound properties*. PhD thesis: Delft University of Technology, 2011.

[13] T.H. Deng and W.G. Knauss. The temperature and frequency dependence of the bulk compliance of poly (vinyl acetate). A re-examination. *Mechanics of time-dependent materials*, 1:33–49, 1997.

[14] J. Diani, P. Gilormini, C. Fredy, and I. Rousseau. Prediciting thermal shape recovery of crosslinked polymer networks from linear viscoelasticity. *Int. J. Solids Struct.*, 49:793–799, 2012.

[15] R. Dudek, M. Scherzer, A. Schubert, and B. Michel. FE-simulation for polymeric packaging materials. *IEEE Trans. on components packaging and manufacturing technology. Part A*, 21:301–309, 1998.

[16] F. Farzbod and M.J. Leamy. Analysis of Bloch's method in structures with energy dissipation. *ASME J. Vibr. Acoust.*, 133:051010, 2011.

[17] J.D. Ferry. *Viscoelastic properties of polymers*. John Wiley and Sons, 1980.

[18] C. Goffaux and J. Sánchez-Dehesa. Two-dimensional phononic crystals studied using a variational method: application to lattices of locally resonant materials. *Phys. Rev. B*, 67:144301, 2003.

[19] M.I. Hussein. Theory of damped Bloch waves in elastic media. *Phys. Rev. B*, 80:212301, 2009.

[20] M.I. Hussein and M.J. Frazier. Band structure of phononic crystal with general damping. *J. Appl. Phys.*, 108:093506, 2010.

[21] M.I. Hussein and M.J. Frazier. *Acoustic metamaterials and phononic crystals*, chapter 6: Damped phononic crystals and acoustic metamaterials. Springer: Berlin, Heidelberg, 2013.

[22] M.I. Hussein and M.J. Frazier. Metadamping: An emergent phenomenon in dissipative metamaterials. *J. Sound Vibr.*, 332:4767–4774, 2013.

[23] M.I. Hussein, M.J. Leamy, and M. Ruzzene. Dynamics of phononic materials and structures: historical origins, recent progress, and future outlook. *Appl. Mech. Rev.*, 66:040802, 2014.

[24] J.D. Joannopoulos, S.G. Johnson, J.N. Winn, and R.D. Meade. *Photonic crystals: molding the flow of light*. Princenton University Press, New Jersey, 2008.

[25] M.S. Kiasat. *Curing shrinkage and residual stresses in viscoelastic thermosetting resisns and composites*. PhD thesis, 2000.

[26] A.O. Krushynska, V.G. Kouznetsova, and M.G.D. Geers. Towards optimal design of locally resonant acoustic metamaterials. *J. Mech. Phys. Solids*, 71:179–196, 2014.

[27] R.S. Lakes. *Viscoelastic materials*. Cambridge University Press, 2009.

[28] H. Leaderman. *Rheology*. New York, 1958.

[29] F. Lemoult, M. Fink, and G. Lerosey. Acoustic resonators for far-field control of sound on a subwavelength scale. *Phys. Rev. Lett.*, 107:064301, 2011.

[30] F. Lemoult, M. Fink, and G. Lerosey. Far-field sub-wavelength imaging and focusing using a wire medium based resonant metalens. *Wave Random Complex*, 21:614–627, 2011.

[31] F. Lemoult, M. Fink, and G. Lerosey. A polychromatic approach to far-field superlensing at visible wavelengths. *Nat. Commun.*, 3:889, 2012.

[32] F. Lemoult, N. Kaina, M. Fink, and G. Lerosey. Wave propagation and control at the deep subwavelength scale in metamaterials. *Nature Phys.*, 9:55–60, 2013.

[33] F. Lemoult, G. Lerosey, J. de Rosny, and M. Fink. Resonant metalenses for breaking the diffraction barrier. *Phys. Rev. Lett.*, 104:203901, 2010.

[34] Z. Liu, C. Chan, and P. Sheng. Three-component elastic wave band-gap material. *Phys. Rev. B*, 65:165116, 2002.

[35] Z. Liu, C. Chan, and P. Sheng. Analytical model of phononic crystals with local resonances. *Phys. Rev. B*, 65:014103, 2005.

[36] Z. Liu, X. Zhang, Y. Mao, Y. Zhu, Z. Yang, C. Chan, and P. Sheng. Locally resonant sonic materials. *Science*, 289:1734–1736, 2000.

[37] H. Lu, X. Zhang, and W.G. Knauss. Uniaxial, shear, and poisson relaxiation and their conversion to bulk relaxation: studies on poly(methyl methacrylate). *Polym. Compos.*, 18:211–222, 1997.

[38] E. Manconi and B.R. Mace. Estimation of the loss factor of viscoelastic laminated panels from finite element analysis. *J. Sound Vib.*, 329:3928–3939, 2010.

[39] J.M. Manimala and C.T. Sun. Microstructural design studies for locally dissipative acoustic metamaterials. *J. Appl. Phys.*, 115:023518, 2014.

[40] D. Mead. A general theory of harmonic wave propagation in linear periodic systems with multiple coupling. *J. Sound Vibr.*, 27:235–260, 1973.

[41] D.J. Mead and S. Markus. Coupled flexural-longitudinal wave motion in a periodic beam. *J. Sound Vib.*, 90:1–24, 1983.

[42] B. Merheb, P.A. Deymier, M. Jain, M. Aloshyna-Lesuffleur, S. Mohanty, A. Berker, and R.W. Greger. Elastic and viscoelastic effects in rubber/air acoustic band gap structures: a theoretical and experimental study. *J. Appl. Phys.*, 104:064913, 2008.

[43] R.D. Mindlin. *An introduction to the mathematical theory of vibrations of elastic plates*. World Scientific, 2006.

[44] R.P. Moiseyenko and V. Laude. Material loss influence on the complex band structure and group velocity in phononic crystals. *Phys. Rev. B*, 83:064301, 2011.

[45] S. Mukherjee and E. Lee. Dispersion relations and mode shapes for waves in laminated viscoelastic composites by finite difference methods. *Compt. Struct.*, 5:279–285, 1975.

[46] M. Oudich, B. Djafari-Rouhani, Y. Pennec, M. B. Assouar, and B. Bornello. Negative effective mass density of acoustic metamaterial plate decorated with low frequency resonant pillars. *J. Appl. Phys.*, 116:184504, 2014.

[47] Y. Pennec, J.O. Vasseur, B. Djafari-Rouhani, L. Dobrzy'nski, and P.A. Deymier. Two-dimensional phononic crystals: examples and applications. *Surface Sci. Rep.*, 65:229–291, 2010.

[48] A. S. Phani and M.I. Hussein. Analysis of damped Bloch waves by the Rayleigh perturbation method. *ASME J. Vibr. Acoust.*, 135:041014, 2013.

[49] S.B. Sane and W.G Knauss. The time-dependent bulk response of poly (methyl methacrylate). *Mech. Time-Depend. Mater.*, 5:293–324, 2001.

[50] T.L. Smith, K. Rao, and I. Dyer. Attenuation of plate flexural waves by a layer of dymanic absorbers. *Noise Control Eng. J.*, 26:56–61, 1986.

[51] T. Still, M. Oudich, G.K. Auerhammer, D. Vlassopoulos, B. Djafari-Rouhani, G. Fytas, and P. Sheng. Soft silicone rubber in phononic structures: correct elastic moduli. *Phys. Rev. B*, 88:094102, 2013.

[52] D.J. Thompson. A continuous damped vibration absorber to reduce broadband wave propagation in beams. *J. Sound Vib.*, 311:824–842, 2008.

[53] N.W. Tschoegl, W.G. Knauss, and I. Emri. Poisson's ratio in linear viscoelasticity - a critical review. *Mech. Time-Depend. Mater.*, 6:3–51, 2001.

[54] J.O. Vasseur, P.A. Deymier, A. Sukhovich, B. Merheb, A.-C. Hladky-Hennion, and M.I. Hussein. *Acoustic metamaterials and phononic crystals*, chapter 10: Phononic band structures and trasmission coefficients: methods and approaches. Springer: Berlin, Heidelberg, 2013.

[55] I.A. Veres, T. Berer, and O. Matsuda. Complex band structures of two dimensional phononic crystals: analysis by the finite element method. *J. Appl. Phys.*, 114:083519, 2013.

[56] P. Wang, F. Casadei, S. Shan, J.C. Weaver, and K. Bertoldi. Harnessing buckling to design tunable locally resonant acoustic metamaterials. *Phys. Rev. Lett.*, 113:014301, 2014.

[57] D.V. Widder. *The Laplace Transform. Princeton Mathematical Series*, volume 6. Princeton University Press, 1941.

[58] Y. Wu, Y. Lai, and Z. Zhang. Effective medium theory for elastic metamaterials in two-dimensions. *Phys. Rev. B*, 76:205313, 2007.

[59] B. Yuan, V.F. Humphrey, J. Wen, and X. Wen. On the coupling of resonance and Bragg scattering effects in three-dimensional locally resonant sonic materials. *Ultrasonics*, 53:1332–1343, 2013.

[60] Y.P. Zhao and P.J. Wei. The band gap of 1D viscoelastic phononic crystal. *Comput. Mater. Sci.*, 46:603–606, 2009.

[61] X. Zhou and G. Hu. Dynamic effective models of two-dimensional acoustic metamaterials with cylindrical inclusions. *Acta Mech.*, 224:1233–1241, 2013.

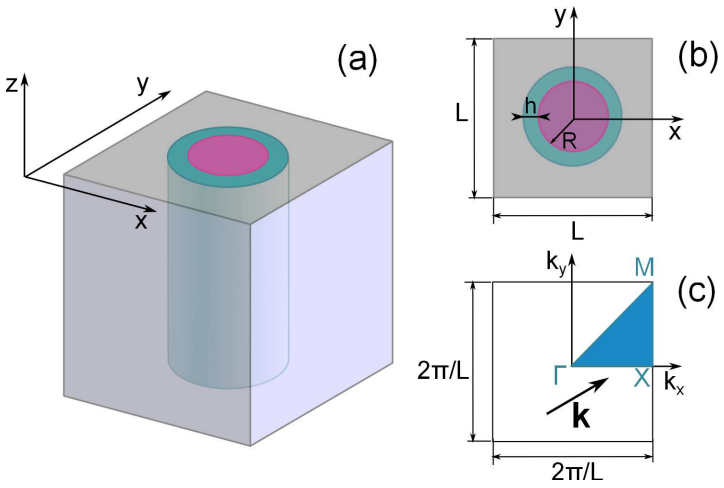

Figure 1: (a) A representative unit cell of an AMM with a square lattice of coated inclusions. The metamaterial is assumed to be infinite along the z axis; (b) 2D cross-section of the metamaterial unit cell; (c) sketch of the corresponding 1st and irreducible Brillouin zones (shaded triangle).

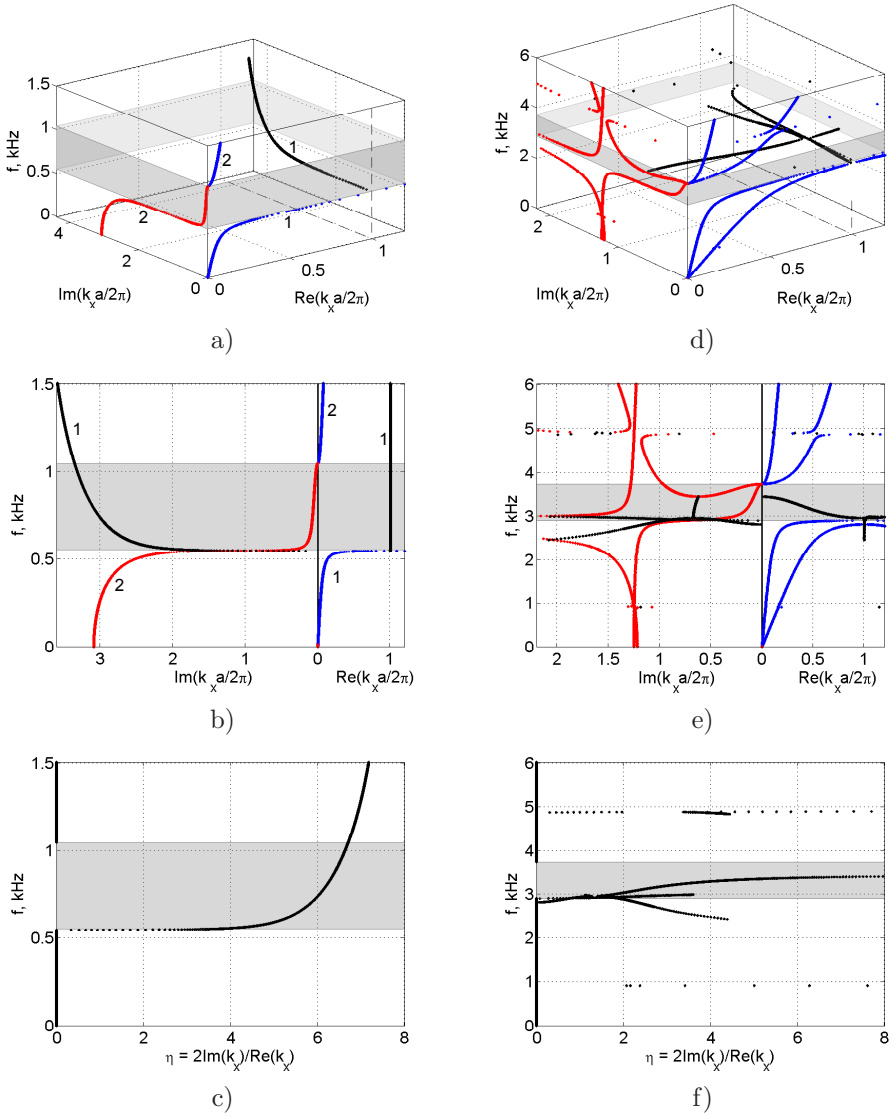

Figure 2: Band structure (a,b,d,e) and attenuation (c,f) diagrams for (a-c) out-of-plane and (d-f) in-plane modes in an undamped linear elastic AMM represented by a unit cell shown in Fig. 1. The geometric parameters are R_{in}=5 mm, h=2.5 mm, and filling fraction of the coated inclusion is 40%. Real, pure imaginary, and complex branches are indicated by blue, red, and black lines, respectively. The boundary of the IBZ for Rek_x is indicated by a black dashed line.

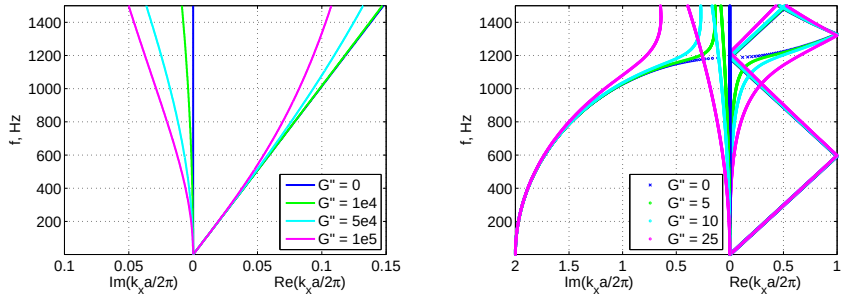

a) b)

Figure 3: Band structures for out-of-plane modes in an empty-lattice viscoelastic a) epoxy and b) rubber material for several values of the shear viscosity G'' in [Pa/s] in the Kelvin-Voigt model (27).

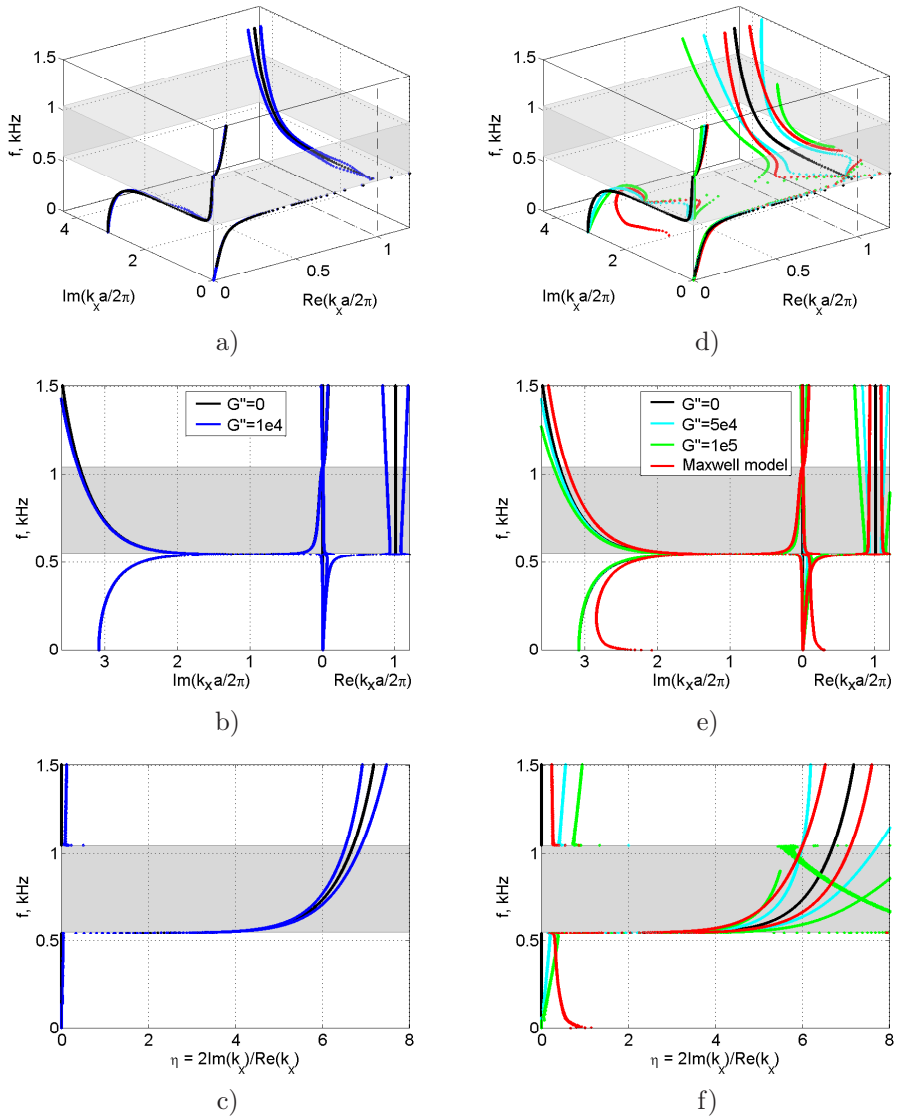

Figure 4: Band structure (a,b,d,e) and attenuation (c,f) diagrams for out-of-plane modes in a dissipative AMM with a damped matrix described by either the Kelvin-Voigt (with various viscosity levels G'' in [Pa·s]) or generalized Maxwell models. The composition of the AMM is the same as in the undamped linear elastic case, with the reference spectrum shown by black lines. The band gap evaluated for the undamped AMM is indicated by gray shaded regions.

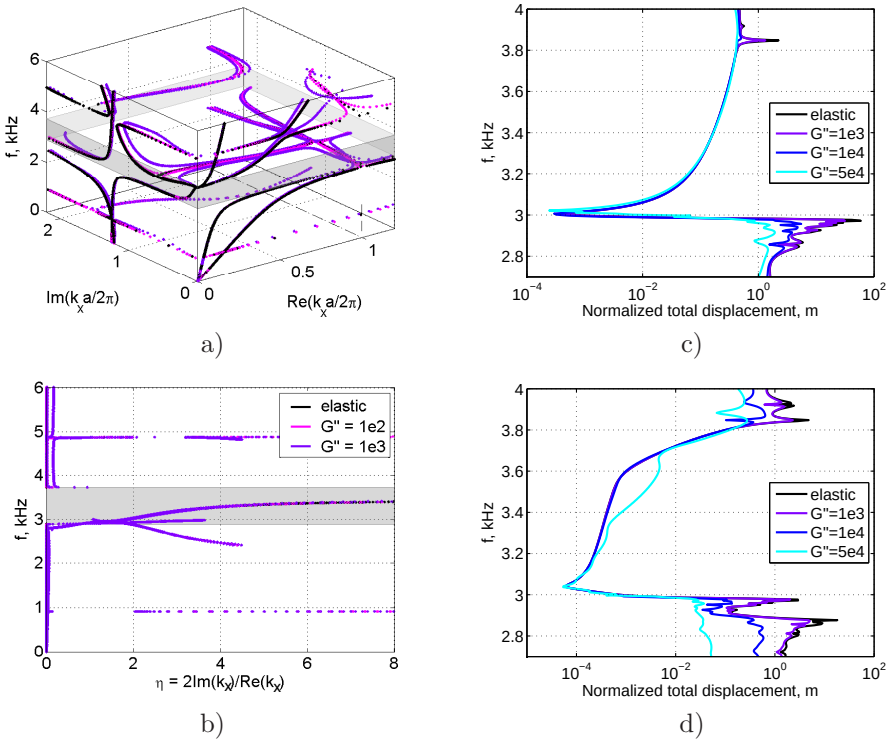

Figure 5: Band structure (a), attenuation (b) and transmission (c,d) diagrams for in-plane modes in a dissipative AMM with damped matrix material described by the Kelvin-Voigt model (with various levels G'' in [Pa·s]). The normalized (to the amplitude of an input wave) transmitted displacements are shown for horizontally (c) and vertically (d) polarized waves. The composition of the AMM is the same as in the undamped linear elastic case with the reference spectrum shown by black lines. The band gap evaluated for the undamped AMM is indicated by gray shaded regions. The transmitted displacements are shown in the vicinity of the band gap frequencies.

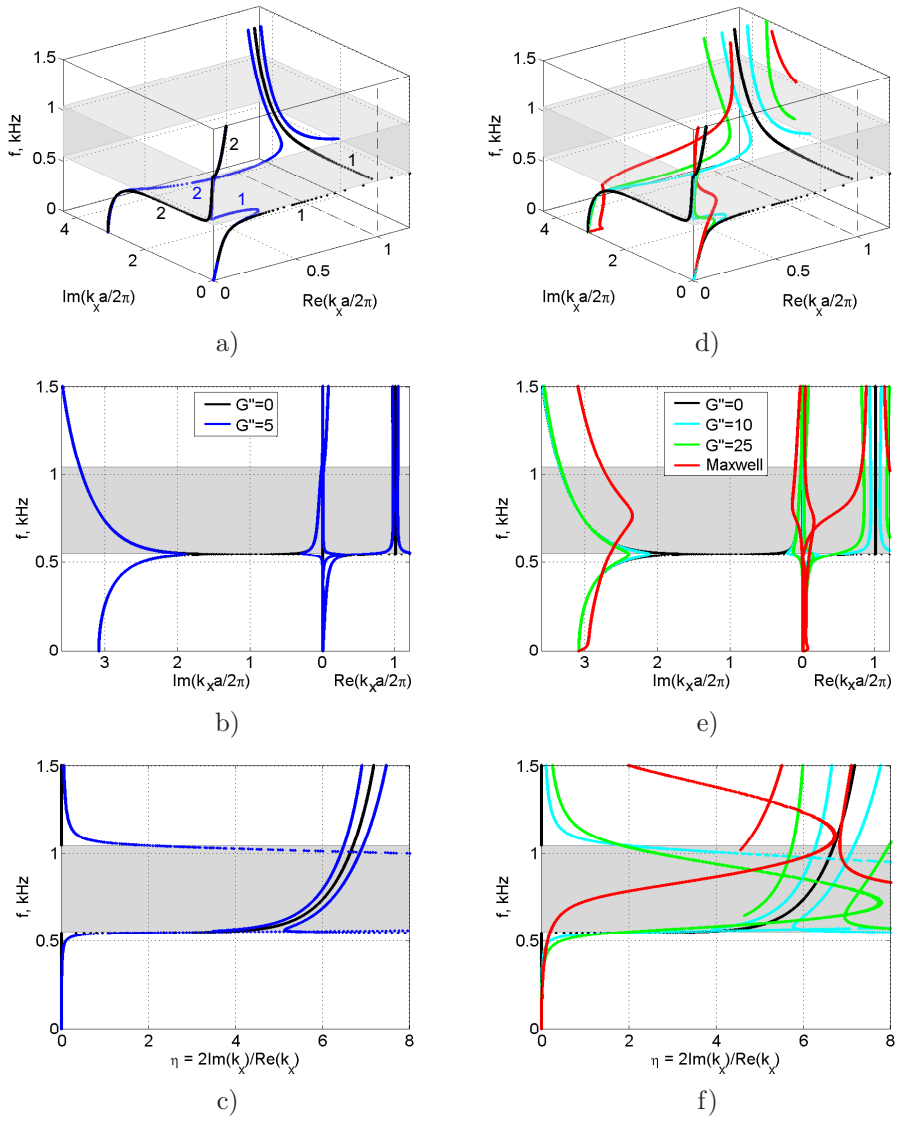

Figure 6: Band structure (a,b,d,e) and attenuation (c,f) diagrams for out-of-plane modes in the dissipative AMM with a damped rubber coating of inclusions described by either the Kelvin-Voigt (with various viscosity levels G'') or the generalized Maxwell model. The composition of the AMM is the same as in the undamped linear elastic case, for which the reference spectrum is shown in black. The band gap evaluated for the undamped AMM is indicated by gray shaded regions.

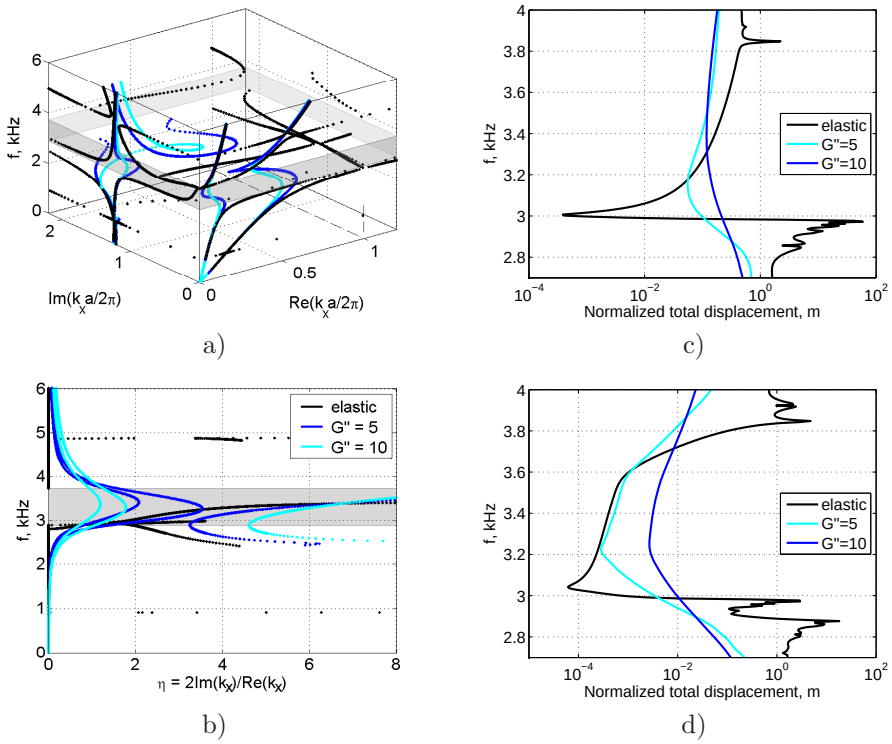

Figure 7: Band structure (a), attenuation (b) and transmission (c,d) diagrams for in-plane modes in a dissipative AMM with damped rubber coating described by the Kelvin-Voigt model with $G'' = 5$ Pa·s (dark blue) and $G'' = 10$ Pa·s (light blue). The normalized (to the amplitude of an input wave) transmitted displacements are shown for horizontally (c) and vertically (d) polarized waves. The composition of the AMM is the same as in the undamped linear elastic case, for which the reference spectrum is indicated by black lines. The band gap evaluated for the undamped AMM is shown by gray shaded regions.

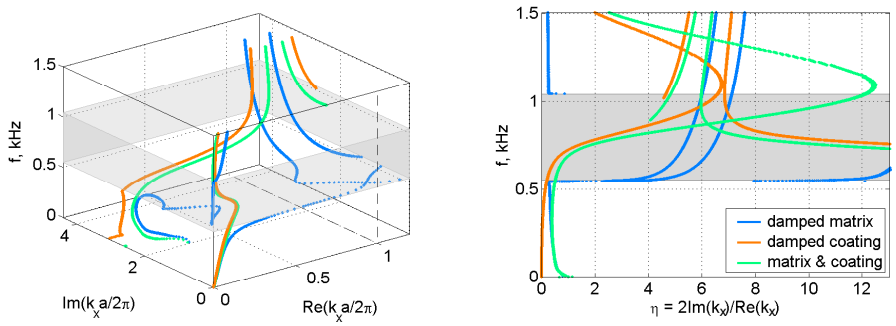

Figure 8: Band structure (a) and attenuation (b) diagrams for the out-of-plane modes in dissipative AMMs with: damped matrix (blue curves), damped coating (orange curves), and damped both matrix and coating (green curves) described by the generalized Maxwell model. The composition of the AMM is the same as in an undamped linear elastic case with the corresponding band gap indicated by gray shaded regions.